ChemPubSoc Europe

DOI: 10.1002/celc.201700109

CHEMELECTROCHEM Articles

NH_3 Post-Treatment Induces High Activity of Co-Based Electrocatalysts Supported on Carbon Nanotubes for the Oxygen Evolution Reaction

Fengkai Yang,[a] Wei Xia,[a] Artjom Maljusch,[b] Justus Masa,[b] Dirk Hollmann,[c] Ilya Sinev,[d] Beatriz Roldan Cuenya,[d] Wolfgang Schuhmann,*[b] and Martin Muhler*[a]

Cobalt oxide nanoparticles were deposited on nitrogen-doped carbon nanotubes (NCNTs) through impregnation by using cobalt nitrate as a precursor and subsequent drying and calcination. Co loadings were prepared in the range from 4 to 40 wt%, and hydrogen and ammonia were applied in the thermal post-treatment of the CoO_x/NCNT samples. The Co_3O_4 spinel structure was detected in all samples, while the thermal treatment in ammonia and hydrogen led to the formation of CoO and metallic Co in addition. Treatment in ammonia resulted in the partial reduction of Co_3O_4 to CoO and nitrogen doping of the oxides, leading to excellent electrocatalytic activity in the oxygen evolution reaction (OER) and stability despite of the lower Co oxidation states compared with the sample calcined in air. In contrast, the sample reduced in hydrogen showed a lower activity and stability in the OER. The high activity of the ammonia-treated sample can be assigned to improved conductivity, favorable surface properties with surface nitrogen improving the hydrophilicity of the catalysts, and the more facile transformation to the OER-active layered cobalt oxyhydroxide phase under anodic conditions.

1. Introduction

Electrochemical energy storage is widely recognized as the most promising solution coping with the fluctuation of power generation from renewable sources. In addition to the popular battery technologies, which suffer from low energy density and limited cycle life,[1] electrolyzers can convert the excess energy into hydrogen and concomitant oxygen.[2] While hydrogen is the chemical storage molecule of interest, the bottleneck of electrochemical water splitting is the oxygen evolution reaction (OER), which typically requires four-electron transfer and a large overpotential.[3] Rutile-type Ir and Ru dioxide have been intensively investigated in recent years and proven to be currently the most active catalysts for OER both theoretically[4] and experimentally.[5] However, the high cost and rare abundance of Ir and Ru as noble metals limit their large-scale applications.

Recently, transition metal-based catalysts such as Mn and Co oxides have attracted enormous interest as low-cost alternatives to noble-metal catalysts for the OER.[6–9] However, these semiconducting oxides have high electrical resistance and cannot be used as electrocatalysts without conductive additives. Typically, carbon materials like carbon black,[10] graphene[7,11] and carbon nanotubes (CNTs)[8,9,12] used as support or conductive additives can improve the conductivity of the electrodes to a sufficiently high level for electrocatalysis. In particular, N-doped carbon materials have been widely used not only to promote electron transfer but also to serve as complementary sites for electrocatalysis.[13] Dai and co-workers reported that cobalt oxide supported on N-doped graphene[7] and spinel manganese-cobalt oxide supported on N-doped reduced graphene oxide[7] can be used for both ORR and OER.

To achieve a high electrical conductivity of electrodes based on semiconducting transition metal oxides as catalysts, a strong coupling between the oxide nanoparticles and the carbon materials as support is highly desirable. Conversely, insufficient contact between metal oxides and carbon often leads to high contact resistance and thus higher Ohmic losses lowering the overall activity. Moreover, the surface oxygen groups on carbon materials, that are often indispensable for the deposition of metal precursors during catalyst synthesis, may be detrimental for the conductivity of the obtained catalysts. While the removal of these oxygen species, for example, by thermal treatment under reducing conditions, improves the conductivity, an appropriate hydrophilicity is lost due to the elimination of surface oxygen, which is needed for the wetting of the catalyst by the electrolyte in three-phase reactions such as the OER.

[a] F. Yang, Dr. W. Xia, Prof. M. Muhler
Laboratory of Industrial Chemistry
Ruhr-University Bochum
Universitätsstr. 150, D-44780 Bochum, Germany
E-mail: muhler@techem.rub.de
[b] Dr. A. Maljusch, Dr. J. Masa, Prof. W. Schuhmann
Analytical Chemistry and Center for Electrochemical Science
Ruhr-University Bochum, Germany
Universitätsstr. 150, D-44780 Bochum
E-mail: wolfgang.schuhmann@rub.de
[c] Dr. D. Hollmann
Leibniz-Institut für Katalyse e.V. (LIKAT)
Albert-Einstein-Str. 29a, 18059 Rostock, Germany
[d] Dr. I. Sinev, Prof. B. R. Cuenya
Department of Physics
Ruhr-University Bochum, Germany
Universitätsstr. 150, D-44780 Bochum

Supporting information for this article is available on the WWW under https://doi.org/10.1002/celc.201700109

An invited contribution on Sustainable Hydrogen (SusHy)

In this work, we propose a synthesis route that tackles all the three major problems of OER electrocatalysts simultaneously: conductivity, hydrophilicity and activity. Cobalt oxide nanoparticles supported on nitrogen-doped CNTs (NCNTs) were synthesized and their OER activity under alkaline conditions was considerably improved by a thermal post-treatment in ammonia.

2. Results and Discussion

Purified NCNTs synthesized by catalytic chemical vapor deposition[14,15] were used as support for Co oxide nanoparticles, which were synthesized by impregnation using Co nitrate followed by drying and calcination. Two series of samples were prepared for comparison: First, the loading of Co was varied by preparing three samples with low (L, about 4 wt%), medium (M, about 20 wt%) and high (H, about 40 wt%) Co loadings (Table 1). These samples were calcined in diluted oxygen at 300 °C. Second, the sample with optimized Co loading for electrochemical characterization, i.e., CoO_x-M/NCNT, was treated in hydrogen or ammonia to tune the oxidation state of Co and the surface properties of the catalysts. It is worth noting that a significant carbon loss was recorded after the calcination in air at 300 °C. Obviously, the presence of a large amount of defects in NCNTs decreased their chemical stability. Furthermore, cobalt oxide nanoparticles catalyze the gasification of carbon favoring the weight loss of the NCNT support.

Table 1. Co loadings determined by ICP-OES measurements.

Sample	Co loading [wt%]
CoO_x-L/NCNT	4.4
CoO_x-M/NCNT	19.6
CoO_x-H/NCNT	38.3
CoO_x-M/NCNT-H_2	21.5
CoO_x-M/NCNT-NH_3	22.3

XRD was employed to investigate the phase composition of the obtained Co nanoparticles supported on NCNTs. The XRD patterns of the samples with different Co loadings and treated under different atmospheres are shown in Figure 1. All the patterns were processed with background subtraction and subsequent normalization. As shown in Figure 1a, the reflections at around 26° and 42.4° originate from the graphitic structure of the NCNTs, while those at about 18.9°, 31.3°, 36.8°, 44.8°, 59.3° and 65.2° indicate the presence of Co_3O_4. By comparing samples with different Co loadings, it can be seen that the reflections related to the spinel structure of Co_3O_4 sharpened significantly, when the Co loading increased from 4.4 (CoO_x-L/NCNT) to 19.6 wt% (CoO_x-M/NCNT). Obviously, larger crystal domains were formed at higher loadings leading to sharper reflections. Figure 1b shows that the thermal treatment in a reducing atmosphere led to the formation of CoO, although Co_3O_4 still can be detected as indicated by reflections at about 18.9° and 31.3°. The reflections in Figure 1b are significantly broader compared with the sharp reflections in Figure 1a, which indicates that the particles were partially reduced leading to two or more phases in a single particle and consequently smaller crystalline domains. Furthermore, the surface was re-oxidized upon exposure to air after reduction, which further reduced the dimensions of each crystalline domain by forming separate metal/metal oxide domains in the entire particle. The overall results are in good agreement with previous studies.[16] It is known from TPR studies that H_2 reduction at 300 °C leads to the formation of CoO from Co_3O_4.[16] After reduction at 350 °C, the cubic phase of metallic Co was detected at $2\theta = 44.5°$. Although the samples were transferred in air resulting in re-oxidation of the surface of the metallic particles formed during reduction, the core of the particle remained metallic thus giving rise to the reflections of cubic Co^0.[17] Obviously, the H_2-treated sample has a higher degree of reduction compared with the NH_3-treated sample. Interestingly, slight shifts of the CoO reflections to higher 2θ values (CoO(111) $2\theta = 37.0°$) were observed for CoO_x-M/NCNT-NH_3 (inset in Figure 1b), which may be related to nitrogen doping of CoO.[18]

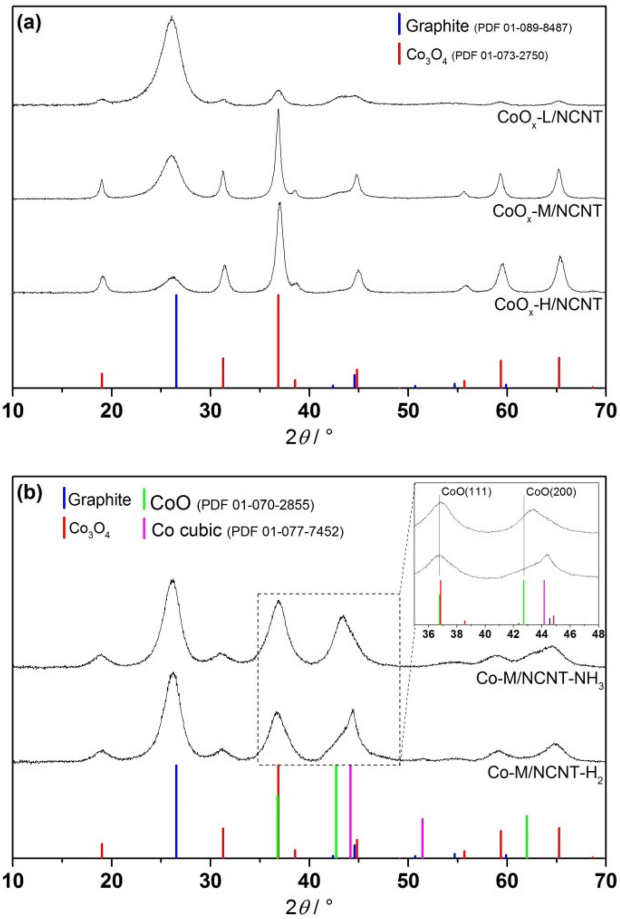

Figure 1. XRD patterns of the samples with a) different Co loadings and b) after post-treatment in NH_3 and H_2.

The structural properties of the samples were further characterized by Raman spectroscopy (Figure 2). It can be seen that all the samples show typical features of carbon materials with two first-order modes at about 1581 cm^{-1} (G-band, E_{2g})

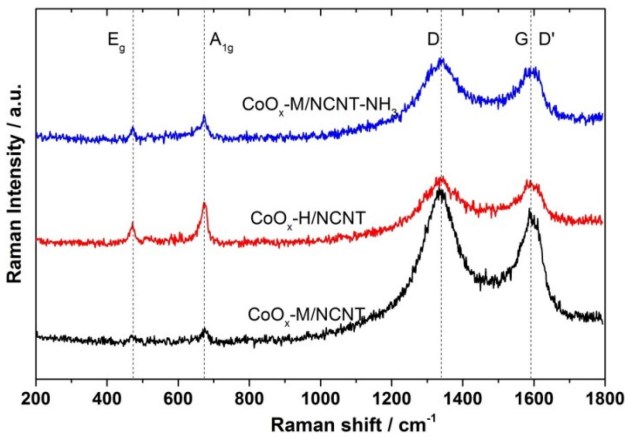

Figure 2. Raman spectra of the CoO_x/NCNT samples.

and 1332 cm^{-1} (D-band, A_{1g}). The shoulder at the high wavenumber side of the G band is related to defects, i.e., the D'-band. The strong D-bands indicate the presence of a large amount of defects, which is typical for NCNTs.[19] At lower wavenumbers, two contributions were detected for all three samples at about 481 and 689 cm^{-1} originating from the E_g and A_{1g} modes of the cobalt oxide spinel. It is known that the A_{1g} mode is related to a vibration that is largely determined by the octahedral cations in the normal spinel, whereas the E_g mode combines the vibration of tetrahedral and octahedral sites.[20] Peak narrowing was observed for the sample with a higher Co loading, but there is no shift of bands indicating that spinel Co_3O_4 is the dominating cobalt oxide phase for all the three samples.

TEM studies confirmed the defective structure of the NCNTs, and the cobalt oxide nanoparticles were found to have diameters mostly between 5–10 nm for all the middle loading samples. As shown in Figure 3, the CoO_x particles are homogeneously distributed on the NCNT support in the CoO_x-M/NCNT-NH3 sample. In comparison to CoO_x-M/NCNT, the post-treatment with NH_3 (300 °C) and H_2 (350 °C) did not cause significant sintering of CoO_x, which is in agreement with our earlier studies where sintering was only detected after treatment at 500 °C in NH_3 and H_2.[21]

The aim of the NH_3 post-treatment was to dope the CoO_x nanoparticles and the carbon surface with N atoms resulting in nitrogen-doped CoO_x and additional surface nitrogen species on the NCNTs. To understand the nitrogen-doping process and to determine the most suitable temperature for the NH_3 treatment, NH_3 decomposition experiments were performed using reference materials. 50 mg of commercial Co_3O_4 and commercial CoO were heated with a ramp of 5 K/min in 100 NmL/min of 4000 ppm NH_3/He (Figure 4). The quantified NH_3 uptake and corresponding NH_3:Co ratios for the tested samples are summarized in Table 2. As shown in Figure 4, commercial CoO consumed a small amount of NH_3 between 210 and 285 °C prior to full catalytic decomposition of NH_3 at 360 °C. It is known from the XRD results (Figure 1b) that CoO cannot be reduced by NH_3. Quantitative analysis disclosed that CoO consumed only a very small amount of NH_3 (Table 2). The

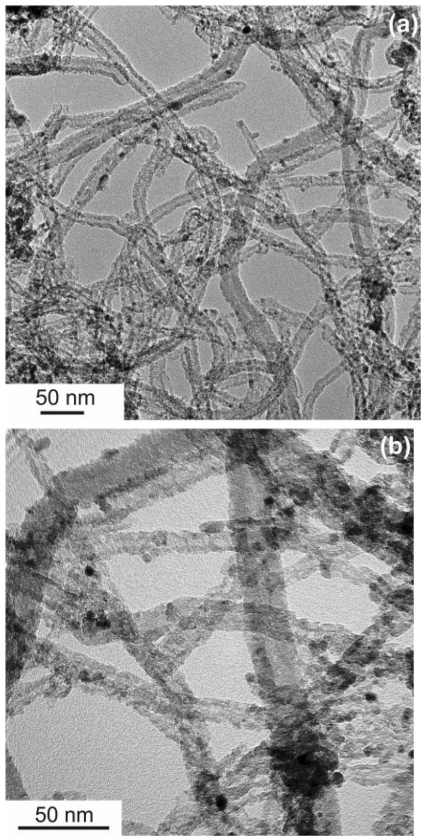

Figure 3. a,b) TEM images of CoO_x-M/NCNT-NH_3 using different magnifications.

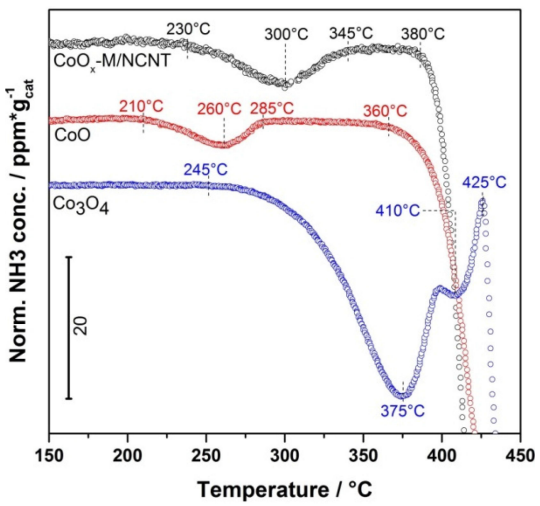

Figure 4. NH_3 decomposition in 100 NmL/min 4000 ppm NH_3/He at a heating rate of 5 K/min with CoO_x-M/NCNT, commercial CoO and commercial Co_3O_4.

Table 2. NH_3 uptake determined by NH_3 decomposition experiments and corresponding molar ratio against Co atoms.

Sample	NH_3 uptake [mmol/g_{cat}]	NH_3/Co ratio
CoO_x-M/NCNT	0.27	1:12.5
Commercial CoO	0.13	1:104.6
Commercial Co_3O_4	1.86	1:6.7

consumption can be tentatively assigned to surface reduction. In comparison, much higher NH_3 consumption was recorded for Co_3O_4 as indicated by two strong uptake peaks at 375 °C and 410 °C, confirming the bulk reduction to CoO. It is worth noting that the NH_3:Co ratio of 1:6.7 is smaller than the theoretical ratio of 1:4.5 needed for the full reduction to CoO. Obviously, the reduction time was not sufficient during the linear heating process.

Figure 4 also includes the NH_3 profile obtained with 20 mg CoO_x-M/NCNT. It can be seen that full catalytic NH_3 decomposition started at about 380 °C, and a further increase in temperature led to a sharp decrease of the NH_3 concentration to zero. Prior to full decomposition, NH_3 uptake was observed in the temperature range of 230–345 °C, which can be correlated to the surface reduction by NH_3 leading to nitrogen doping. The onset temperature (230 °C) of CoO_x-M/NCNT is lower than that of pure Co_3O_4 (245 °C). These results confirm that 300 °C is a suitable temperature for NH_3 treatment and N-doped CoO is the most favorable product under these conditions. Compared with the Co_3O_4 reference, CoO_x-M/NCNT possesses more CoO-like properties concerning the onset temperature, the uptake peak temperature as well as the NH_3:Co ratio suggesting a lower oxidation states of the CoO_x nanoparticles than bulk Co_3O_4 on the NCNT support. This observation is in good agreement with our previous studies demonstrating that NCNTs favor the formation of metal species in lower oxidation states due to metal-nitrogen bonding.[22]

The samples treated in different atmospheres were investigated further by XPS to analyze the influence on the oxidation state. It can be seen from Figure 5a that the Co $2p_{3/2}$ XP spectra increase in intensity by a factor of 2 after the treatment in both H_2 and NH_3. This increase can be related to the removal of carbonaceous species from the surface of the CoO_x nanoparticles by the thermal treatments. The carbon deposits are assumed to originate from the calcination in air, which resulted in a strong weight loss. Table 3 shows the surface atomic compositions derived from the XPS measurements, which confirm the strong increase of CoO_x. A closer look at the Co $2p_{3/2}$ main line and its satellites (see supporting information for the detailed analysis, Table SI1) indicates the predominance of Co-N_x and Co(III) species in the calcined sample, which are partially transformed to Co(II) species due to the H_2 and NH_3 treatments.[23] It must be pointed out that there were no hints of metallic Co detected even after reduction in hydrogen, most likely due to transfer in air to the XPS system after the reductive treatment.

The N 1 s XP spectra in Figure 5b consist of 4 major contributions at 398.5, 400.0, 401.1 and 402.7 eV, which agree rather well with values reported for pyridinic, N_x-Co nitrogen species, pyrrolic and quarternary/graphitic N.[24] The reduction in H_2 led to a significant depletion of nitrogen observed by XPS accompanied by a decrease of the relative amount of N_x-Co and graphitic nitrogen species. Treatment in NH_3, in contrast, did not result in a significant change of the nitrogen concentration in the near surface region, but, similarly to the H_2-treated sample led to a lower fraction of N_x-Co, graphitic as well as pyrrolic nitrogen species (see supporting information for further details, Table SI2).

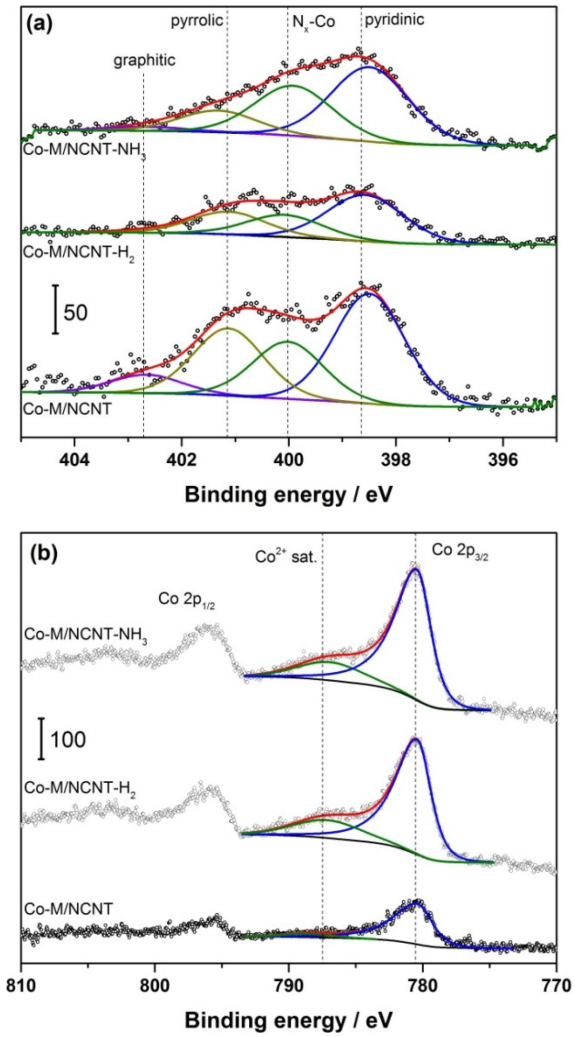

Figure 5. XPS spectra of the a) N 1 s and b) Co 2p regions of the calcined CoO_x-M/NCNT samples further treated in H_2 and NH_3.

Table 3. Surface atomic concentrations derived by XPS.

Sample	C	O	N	Co
CoO_x-M/NCNT	88.1	5.3	5.3	1.3
CoO_x-M/NCNT-H_2	83.9	10.6	2.9	2.6
CoO_x-M/NCNT-NH_3	82.9	10.3	4.3	2.5

Although XPS did not show any significant difference in the state of Co after thermal treatment in H_2 and NH_3 in the near-surface region, ex-situ X-ray absorption near edge structure (XANES) measurements at the Co *K*-edge showed striking changes in the Co oxidation state and local coordination in the bulk. The XANES spectrum of the calcined CoO_x-M/NCNT sample did not show any close resemblance to the Co references measured (Figures 6a and 6b, respectively). It has a broad pre-edge peak at 7707.3 eV and a broad feature above the edge with a small peak at 7728.3 eV. The latter is close the maximum of the peak observed for Co_3O_4 (7729 eV, so-called

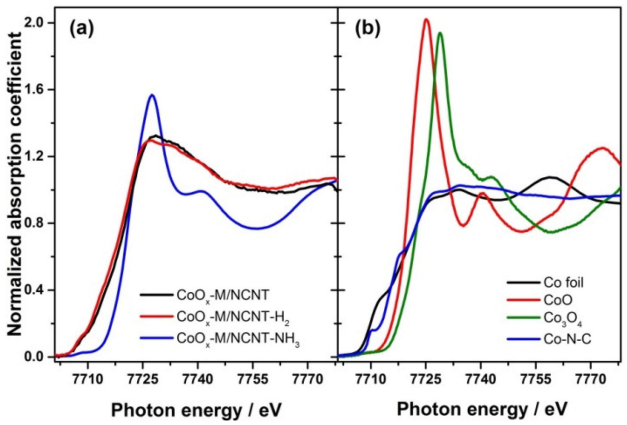

Figure 6. XANES spectra of calcined CoO_x-M/NCNT samples further treated in H_2 and NH_3 (a) and various Co reference compounds (b).

"white line"), although it is nowhere close in intensity. The Co *K*-edge XANES represents 1s–3d (pre-edge) and 1s–4p (white line) transitions guided by selection rules and strongly depends on the geometry of the local environment of the Co atoms. The discrepancy between the XANES spectra of the calcined CoO_x-M/NCNT sample and available reference compounds along with the XRD and Raman results suggest the presence of a significant amount of Co species lacking long-range order to give any detectable XRD signal, as expected for a disordered Co-N_x phase in the sample. The XANES spectrum of the CoO_x-M/NCNT-H_2 sample resembles that of the calcined sample with the absorption edge slightly shifted towards lower photon energies, which is generally accepted as an evidence of a slightly less oxidized state. XANES linear combination fitting analysis using spectra of available reference compounds and the calcined sample suggest the presence of a small amount of metallic cobalt in that sample (Figure SI1, Table SI3). The XANES spectrum of the sample treated in NH_3 is remarkably different from the two previously described samples. Its general shape resembles that of CoO and Co_3O_4 with a weak pre-edge feature at 7708.9 eV, an intense white line at 7727.8 and a second post-edge feature at 7741.4 eV. Both the edge position and spectral features are shifted towards higher photon energy compared with CoO and towards lower energy compared with Co_3O_4, suggesting a mixture of both CoO and spinel Co_3O_4 structures. Indeed, a linear combination fitting analysis suggests 31.5% of CoO, 54% Co_3O_4 along with 11% of Co-porphyrin and traces of CoO_x-M/NCNT (Figure SI1, Table SI3).

It must be pointed out, however, that none of the samples showed a characteristic pre-edge feature typical for chemical compounds with Co-N_x coordination between 7714 and 7717 eV in XAFS,[25] which was also observed in our previous study of a Co_xO_y/NC catalyst comprised of CoO_x and Co-N_x groups embedded in a N-doped carbon matrix.[10] The presence of Co-N_x species is, however, suggested by both the N 1 s and Co $2p_{3/2}$ XP spectra, leading to the conjecture that the major amount of Co-N_x coordination is at the surface of the nanoparticles, while their core is comprised of cobalt oxides. It is also consistent with the conclusions from the NH_3 decomposition experiments using the CoO_x-M/NCNT-NH_3 sample, where NH_3 decomposition and the N-doping process were found to take place predominantly on the CoO_x surface.

The electrochemical performance of the samples was evaluated by rotating disc voltammetry, and the results are shown in Figure 7. For the samples with the same calcination

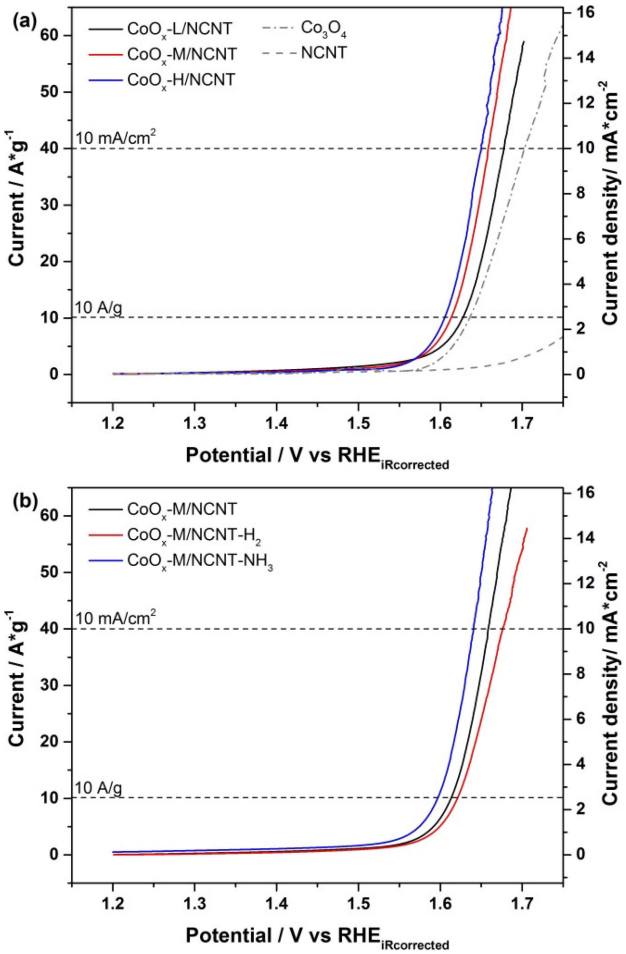

Figure 7. OER activities for the different CoO_x/NCNT catalysts a) calcined in oxygen with different Co loadings and b) further post-treated under different atmospheres.

conditions, the OER current showed a clear increase with increasing Co loading, although the onset potentials seem to be similar (Figure 7a). On the other hand, the reduction treatment in H_2 led to a higher overpotential and a lower activity (Figure 7b). In comparison, the post-treatment in NH_3, which is also reducing, resulted in a clear increase in the OER activity as indicated by the decreased onset potential. This improvement can be related to the improved conductivity of CoO_x due to the NH_3 treatment. In addition, the presence of surface nitrogen groups improves the hydrophilicity of the catalysts, which impedes the buildup of gas bubbles and is beneficial for their release from the electrode surface during the OER. More importantly, the CoO_x nanoparticles in lower oxidation states, which are stabilized by the nitrogen-containing groups present on pristine NCNT and additionally generated

by the NH_3 treatment, are obviously favorable for the transformation to the OER-active layered cobalt oxyhydroxide under anodic conditions, as suggested by recent state-of-the-art studies on the active phase of CoO_x-based OER catalysts.[26]

A thorough quantitative analysis of the electrocatalytic results is presented in Table 4 with all relevant experimental details. Among others, the current at 1.6 V and the potential at 10 A/g were listed for all the samples. The onset potentials appear at around 1.55 V for all the samples. However, the NH_3-treated sample (CoO_x-M/NCNT-NH_3) has an almost doubled current of 12.127 A/g at 1.6 V and a significantly lower potential of 1.594 V at 10 A/g compared with other samples pointing to its superior OER activity induced by the NH_3 treatment. The outstanding performance of CoO_x/NCNT in relation to the Co_3O_4 reference is mostly ascribed to electronic coupling between CoO_x and the NCNTs leading to faster charge transfer across the CoO_x/NCNT-electrolyte interface as probed by electrochemical impedance spectroscopy (EIS, Figure SI2), where the charge transfer resistance was found to be lowered from about 750 Ω to 120 Ω. Additionally, the stability of the samples was evaluated by galvanostatic measurements at 1.6 A/g for 900 s. As shown in Figure 8a, the initial and final potentials as well as degradation rates decreased with increasing Co loadings indicating that higher activity and stability can be achieved by higher Co loadings. The NH_3-treated sample exhibited a lower initial and final potential and similar degradation rate (9.3 μV/s) compared with the untreated sample (8.9 μV/s). This result disclosed that the NH_3 treatment enhanced the activity rather than the stability. In comparison, the H_2-treated sample showed much higher potentials and a higher degradation rate of 25.0 μV/s. Moreover, the CoO_x-M/NCNT-NH_3 catalyst was further tested for long-term stability under more harsh conditions on a graphite RDE with a rotation speed of 900 rpm. As shown in Figure 8b, the NH_3-treated sample exhibited superior stability with a potential of about 1.676 V vs. RHE for 45 h at 40 A/g (equivalent to 10 mA/cm^2). These results confirm the main conclusions from the LSV measurements, that is, the sample treated in NH_3 showed a superior electrocatalytic activity and stability (Figure SI3).

Table 4. Electrochemical activity in the OER measured in 0.1 M KOH. Samples with different Co loadings and post-treatments are listed.

Sample[a]	L	M	H	M + NH_3	M + H_2
E_{onset} [V]	1.58	1.56	1.55	1.54	1.56
I@1.6 V [A/g]	4.65	6.33	7.40	12.13	6.73
E@10 A/g [V]	1.63	1.61	1.61	1.59	1.69

[a] V vs. RHE

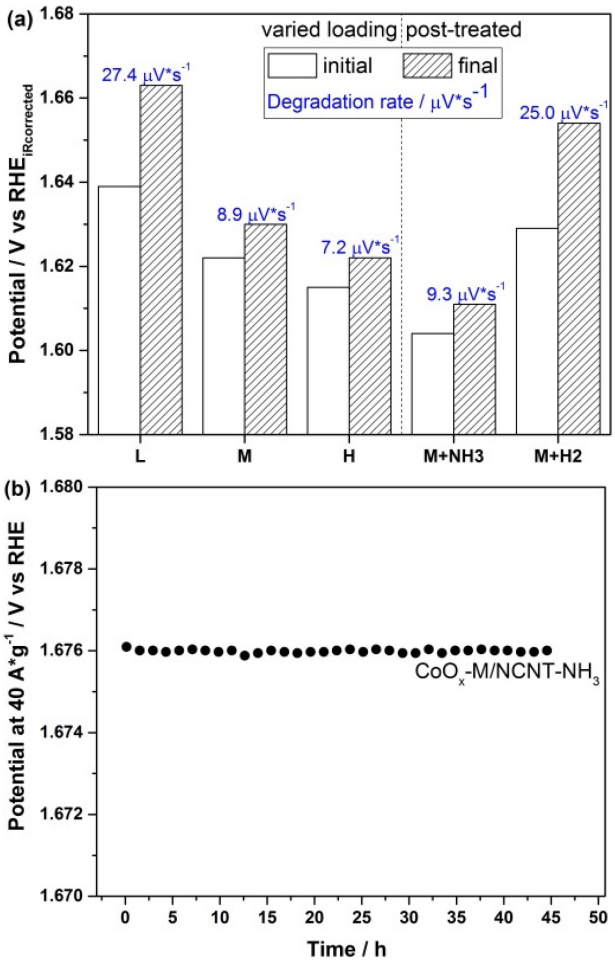

Figure 8. a) Results of galvanostatic stability tests at 10 A/g and degradation rate for the samples with varied Co loadings and different post-treatments. b) Long-term stability of the CoO_x-M/NCNT-NH_3 catalyst as a function of potential with time recorded at a current of 40 A/g in 0.1 M KOH on a graphite RDE electrode maintained at a rotation speed of 900 rpm.

3. Conclusions

Co oxide nanoparticles deposited on NCNTs were investigated as a function of the CoO_x loading and the thermal post-treatment conditions. Co_3O_4 was detected in all the samples after calcination by XRD and Raman spectroscopy, while the thermal post-treatment in ammonia and hydrogen led to the additional formation of CoO and metallic Co. When applied as electrocatalysts, the sample treated in ammonia showed excellent electrocatalytic activity and stability. In contrast, the sample reduced in hydrogen was less active and stable in the OER. The high activity of the ammonia-treated sample is ascribed to nitrogen doping of CoO_x enhancing its conductivity and to the presence of surface nitrogen species on the support improving the hydrophilicity of the catalysts. Furthermore, ammonia decomposition experiments demonstrated the CoO-like nature of the CoO_x nanoparticles stabilized by metal-nitrogen bonds on the ammonia-treated NCNTs, which seems to facilitate the transformation to OER-active cobalt oxyhydroxide under anodic potentials.

Experimental Section

NCNT Preparation and Purification

The nitrogen doped carbon nanotubes used in this study were synthesized by catalytic chemical vapor deposition from a nitrogen-containing precursor. Co-based mixed oxide was used as catalyst for the growth with MnO_x as promoter.[15] The NCNTs were purified to remove the catalyst residues before further synthesis in this work. In a typical process for NCNT purification, 8 g of the as-grown NCNTs were mixed with 800 mL of 1.5 M nitric acid aqueous solution in a 1000 mL beaker. The mixture was kept under stirring for 72 h at room temperature. The NCNTs were then filtrated and re-dispersed in 300 mL deionized water. This process was repeated until the pH of filtrate became neutral. After drying in circulating air at 80 °C for 12 h, the NCNTs were ground in an agate mortar to fine powders for further use.

Preparation of Co-M/NCNT and Post-Treatment

Wet impregnation was used for the preparation with $Co(NO_3)_2{\cdot}6H_2O$ (Sigma-Aldrich, 99.999%) as Co source and purified NCNTs as support. A solution was prepared by dissolving the nitrate of predetermined amount in 50 mL of deionized water. Subsequently, 1 g of the purified NCNTs was added to the solution in a 100 mL round-bottomed flask and the suspension was stirred at room temperature for 2 h. The solvent was then removed in a rotary evaporator by heating the flask at 50 °C under the pressure of 75 mbar. The obtained dark powder was dried in a tubular furnace at 120 °C for 2 h under helium flow (100 NmL/min) to obtain the precursor of the catalyst. After grinding in an agate mortar, the precursor was thermally treated at 300 °C for 90 min in diluted oxygen (5 vol% O_2/He) with a flow rate of 100 NmL/min. Three different cobalt nitrate solutions were prepared by using different amount of $Co(NO_3)_2{\cdot}6H_2O$ including 101, 549 and 1235 mg leading to a theoretical Co loading of 2, 10 and 20 wt%, respectively.

The sample with medium Co loading calcined in 5 vol% oxygen (CoO_x-M/NCNT) was further thermally treated in diluted H_2 (10 vol% H_2/He) or NH_3 (10 vol% NH_3/He), respectively. The treatment in H_2 was performed at 350 °C for 2 h, while the treatment in NH_3 was carried out at 300 °C for 6 h. Typically 200 mg of sample was used in each treatment with a total flow rate of 100 NmL/min.

Characterization

The NH_3 decomposition experiments were performed in a U-shaped quartz tube reactor. 20 mg of the sample CoO_x-M/NCNT was used for the measurement. The reactor with sample was first purged with 100 NmL/min He at 50 °C for 30 min to remove moisture and adsorbed species. NH_3 (4000 ppm in He, 100 NmL/min) was then introduced to the reactor and the sample was heated to 650 °C with a heating rate of 5 K/min. The NH_3 concentration in exhaust gas stream was recorded by an online infrared detector (Bühler Technology, Germany). For comparison, 50 mg commercial CoO and 50 mg commercial Co_3O_4 (Sigma-Aldrich) were tested by the same procedure.

Inductively coupled plasma-optical emission spectroscopy (ICP-OES, PU701 UNICAM) was used to determine the cobalt loadings in different samples. The XRD patterns were recorded in a Philips X'Pert MPD system with the Cu Kα irradiation and post-monochromator in a 2θ range of 10° to 80°. X-ray photoelectron spectroscopy (XPS) measurements were carried out in an ultra-high vacuum (UHV) set-up equipped with a monochromatic Al Kα X-ray source (1486.6 eV; anode operating at 14.5 kV and 45 mA) and a high resolution Gammadata-Scienta SES 2002 analyzer. The base pressure in the measurement chamber was maintained at about 7×10^{-10} mbar. The XP spectra were recorded in the fixed transmission mode with a pass energy of 200 eV resulting in an overall energy resolution better than 0.5 eV. Charging effects were compensated by applying a flood gun.

The X-ray absorption fine structure spectroscopy (XAFS) measurements were performed at the undulator beamline P65 of PETRA III storage ring operating at 6 GeV in top-up mode. The experiments were carried out in transmission mode at the Co*K* (7709 eV) edge. For each of the samples multiple identical spectra were acquired and averaged to improve the signal-to-noise ratio. Initial processing of the XANES data was performed using the program Athena.[27]

Electrochemical Studies

The prepared catalysts were coated on the cleaned surface of a 3.8 mm rotation glassy carbon electrode (GC RDE) via the drop coating method using a catalyst ink. The loadings of electrocatalyst, conducting additive (CA, Vulcan XC-72) and Nafion (alkaline solution in KOH) were kept at 250 μg/cm^2, 50 μg/cm^2 and 50 μg/cm^2 on electrode, respectively. The solvent was made from deionized water and anhydrous ethanol with a ratio of 1:1. After mixing each component, the catalyst ink was homogenized in an ultrasonic bath for 2 h and then directly dropped on the RDE electrodes. The coated electrodes were finally dried overnight in humid atmosphere for further electrochemical tests.

The prepared electrodes were tested in a three-electrode system with Pt mesh as counter electrode, Ag/AgCl 3 M KCl as reference electrode. The electrolyte was 0.1 M KOH saturated with O_2. Electrochemical impedance spectroscopy (EIS) was measured at the open circuit potential (OCP) from 20 Hz to 200 kHz with an AC perturbation of 5 mV to determine the uncompensated resistance. Linear sweep voltammetry (LSV) was carried out between 1.2 V to 1.8 V vs RHE with a scan rate of 1 mV/s under a rotation rate of 400 rpm. The potential in LSV was iR corrected with the uncompensated potential from EIS measurement. The galvanostatic stability test (GSS) was performed under a specific current of 10 A/g for 900 s. Long term stability was investigated by recording a chronopotentiometric curve at a current density of 40 A/g on a graphite RDE electrode maintained at a rotation speed of 900 rpm for 45 h.

Acknowledgements

Financial support (SusHy: Grant 03X3581D) from the German Federal Ministry of Education and Research (BMBF) is gratefully acknowledged. Funding from the Deutsche Forschungsgemeinschaft (DFG) through the Cluster of Excellence RESOLV at RUB is greatly appreciated.

Conflict of Interest

The authors declare no conflict of interest.

Keywords: Co · carbon nanotubes · nitrogen doping · oxygen evolution reaction · ammonia treatment

References

[1] T. R. Cook, D. K. Dogutan, S. Y. Reece, Y. Surendranath, T. S. Teets, D. G. Nocera, *Chem. Rev.* **2010**, *110*, 6474–6502.
[2] S. Park, Y. Shao, J. Liu, Y. Wang, *Energy Environ. Sci.* **2012**, *5*, 9331.
[3] I. Katsounaros, S. Cherevko, A. R. Zeradjanin, K. J. J. Mayrhofer, *Angew. Chem. Int. Ed.* **2014**, *53*, 102–121.
[4] I. C. Man, H.-Y. Su, F. Calle-Vallejo, H. A. Hansen, J. I. Martínez, N. G. Inoglu, J. Kitchin, T. F. Jaramillo, J. K. Nørskov, J. Rossmeisl, *ChemCatChem* **2011**, *3*, 1159–1165.
[5] T. Reier, M. Oezaslan, P. Strasser, *ACS Catal.* **2012**, *2*, 1765–1772.
[6] Y. Gorlin, T. F. Jaramillo, *J. Am. Chem. Soc.* **2010**, *132*, 13612–13614.
[7] Y. Liang, Y. Li, H. Wang, J. Zhou, J. Wang, T. Regier, H. Dai, *Nat. Mater.* **2011**, *10*, 780–786.
[8] A. Zhao, J. Masa, W. Xia, A. Maljusch, M.-G. Willinger, G. Clavel, K. Xie, R. Schlögl, W. Schuhmann, M. Muhler, *J. Am. Chem. Soc.* **2014**, *136*, 7551–7554.
[9] K. Xie, J. Masa, E. Madej, F. Yang, P. Weide, W. Dong, M. Muhler, W. Schuhmann, W. Xia, *ChemCatChem* **2015**, *7*, 3027–3035.
[10] J. Masa, W. Xia, I. Sinev, A. Zhao, Z. Sun, S. Grützke, P. Weide, M. Muhler, W. Schuhmann, *Angew. Chem. Int. Ed.* **2014**, *53*, 8508–8512.
[11] J. Feng, Y. Liang, H. Wang, Y. Li, B. Zhang, J. Zhou, J. Wang, T. Regier, H. Dai, *Nano Res.* **2012**, *5*, 718–725.
[12] Z. Yang, X. Zhou, H. Nie, Z. Yao, S. Huang, *ACS Appl. Mater. & Inter.* **2011**, *3*, 2601–2606.
[13] a) Z. Chen, A. Yu, R. Ahmed, H. Wang, H. Li, Z. Chen, *Electrochim. Acta* **2012**, *69*, 295–300; b) Y. Liang et al., *J. Am. Chem. Soc.* **2012**, *134*, 15849–15857; c) H. Jin, J. Wang, D. Su, Z. Wei, Z. Pang, Y. Wang, *J. Am. Chem. Soc.* **2015**, *137*, 2688–2694;
[14] J.-P. Tessonnier, M. Becker, W. Xia, F. Girgsdies, R. Blume, L. Yao, D. S. Su, M. Muhler, R. Schlögl, *ChemCatChem* **2010**, *2*, 1559–1561.
[15] M. J. Becker, W. Xia, J.-P. Tessonnier, R. Blume, L. Yao, R. Schlögl, M. Muhler, *Carbon* **2011**, *49*, 5253–5264.
[16] P. Chen, F. Yang, A. Kostka, W. Xia, *ACS Catal.* **2014**, *4*, 1478–1486.
[17] D. Banerjee, R. V. Jagadeesh, K. Junge, M.-M. Pohl, J. Radnik, A. Brückner, M. Beller, *Angew. Chem. Int. Ed.* **2014**, *53*, 4359–4363.
[18] H. Yu, Y. Li, X. Li, L. Fan, S. Yang, *Chem. Eur. J.* **2014**, *20*, 3457–3462.
[19] K. Xie, F. Yang, P. Ebbinghaus, A. Erbe, M. Muhler, W. Xia, *J. Energy Chem.* **2015**, *24*, 407–415.
[20] N. Bahlawane, P. H. T. Ngamou, V. Vannier, T. Kottke, J. Heberle, K. Kohse-Höinghaus, *Phys. Chem. Chem. Phys.* **2009**, *11*, 9224–9232.
[21] M. D. Sánchez, P. Chen, T. Reinecke, M. Muhler, W. Xia, *ChemCatChem* **2012**, *4*, 1997–2004.
[22] W. Xia, *Catal. Sci. Technol.* **2016**, *6*, 630–644.
[23] J. Yang, H. Liu, W. N. Martens, R. L. Frost, *J. Phys. Chem. C* **2010**, *114*, 111–119.
[24] a) K. Artyushkova, A. Serov, S. Rojas-Carbonell, P. Atanassov, *J. Phys. Chem. C* **2015**, *119*, 25917–25928; b) J. Casanovas, J. M. Ricart, J. Rubio, F. Illas, J. M. Jiménez-Mateos, *J. Am. Chem. Soc.* **1996**, *118*, 8071–8076; c) A. Zhao, J. Masa, W. Schuhmann, W. Xia, *J. Phys. Chem. C* **2013**, *117*, 24283–24291;
[25] J. C. Swarbrick, T.-C. Weng, K. Schulte, A. N. Khlobystov, P. Glatzel, *Phys. Chem. Chem. Phys.* **2010**, *12*, 9693–9699.
[26] a) J. Bao, X. Zhang, B. Fan, J. Zhang, M. Zhou, W. Yang, X. Hu, H. Wang, B. Pan, Y. Xie, *Angew. Chem. Int. Ed.* **2015**, *54*, 7399–7404; b) L. Trotochaud, J. K. Ranney, K. N. Williams, S. W. Boettcher, *J. Am. Chem. Soc.* **2012**, *134*, 17253–17261; c) C.-W. Tung, Y.-Y. Hsu, Y.-P. Shen, Y. Zheng, T.-S. Chan, H.-S. Sheu, Y.-C. Cheng, H. M. Chen, *Nat. Commun.* **2015**, *6*, 8106; d) L. Xu, Q. Jiang, Z. Xiao, X. Li, J. Huo, S. Wang, L. Dai, *Angew. Chem. Int. Ed.* **2016**, *55*, 5277–5281;
[27] B. Ravel, M. Newville, *J. Synchrotron Radiat.* **2005**, *12*, 537–541.

Manuscript received: January 30, 2017
Accepted Article published: April 19, 2017
Version of record online: May 17, 2017